AFRL-RQ-ED-TR-2017-0012

A Hybrid Model for Multiscale Laser Plasma Simulations with Detailed Collisional Physics

D. Bilyeu

Air Force Research Laboratory (AFMC)
AFRL/RQRS
In-Space Propulsion Branch
1 Ara Drive
Edwards AFB, CA 93524

June 2017

In-House Final Report

AIR FORCE RESEARCH LABORATORY
AEROSPACE SYSTEMS DIRECTORATE

■ Air Force Materiel Command ■ United States Air Force ■ Edwards Air Force Base, CA 93524

- STINFO COPY -
NOTICE AND SIGNATURE PAGE

Using Government drawings, specifications, or other data included in this document for any purpose other than Government procurement does not in any way obligate the U.S. Government. The fact that the Government formulated or supplied the drawings, specifications, or other data does not license the holder or any other person or corporation; or convey any rights or permission to manufacture, use, or sell any patented invention that may relate to them.

Qualified requestors may obtain copies of this report from the Defense Technical Information Center (DTIC) (http://www.dtic.mil).

AFRL-RQ-ED-TR-2017-0012 HAS BEEN REVIEWED AND IS APPROVED FOR PUBLICATION IN ACCORDANCE WITH ASSIGNED DISTRIBUTION STATEMENT.

FOR THE DIRECTOR:

//signed//

DAVID L. BILYEU
Program Manager

//signed//

JUSTIN W. KOO, Ph.D.
Technical Advisor
In-Space Propulsion Branch

//signed//

Technical Advisor
Rocket Propulsion Division

This report is published in the interest of scientific and technical information exchange, and its publication does not constitute the Government's approval or disapproval of its ideas or findings.

REPORT DOCUMENTATION PAGE

Form Approved
OMB No. 0704-0188

1. REPORT DATE *(DD-MM-YYYY)*	**2. REPORT TYPE**	**3. DATES COVERED** *(From - To)*
6/23/2017	In-House Final Report	6/23/2011 - 3/24/2017

4. TITLE AND SUBTITLE
A Hybrid Model for Multiscale Laser Plasma Simulations with Detailed Collisional Physics

5a. CONTRACT NUMBER

5b. GRANT NUMBER

5c. PROGRAM ELEMENT NUMBER
AFOSR; 61102F

6. AUTHOR(S)
D. Bilyeu

5d. PROJECT NUMBER

5e. TASK NUMBER

5f. WORK UNIT NUMBER
Q02Z

7. PERFORMING ORGANIZATION NAME(S) AND ADDRESS(ES)

Air Force Research Laboratory (AFMC)
AFRL/RQRS
1 Ara Drive
Edwards AFB, CA 93524

8. PERFORMING ORGANIZATION REPORT NO.

9. SPONSORING / MONITORING AGENCY NAME(S) AND ADDRESS(ES)

Air Force Research Laboratory (AFMC)
AFRL/RQR
5 Pollux Drive
Edwards AFB, CA 93524

10. SPONSOR/MONITOR'S ACRONYM(S)

11. SPONSOR/MONITOR'S REPORT NUMBER(S)
AFRL-RQ-ED-TR-2017-0012

12. DISTRIBUTION / AVAILABILITY STATEMENT
Approved for public release; distribution unlimited

13. SUPPLEMENTARY NOTES
PA Clearance #: 17399

14. **ABSTRACT**
The purpose of this document is to summarize the work accomplished under work unit Q02Z. The sole source of funding for this program was through AFOSR and was supported by Dr. Jason Marshall under contract 14RQ05COR and Dr. Fariba Fahroo under contract 12RZ06COR.

The goal of this project was to develop a new numerical approach for multiscale plasma simulations that spans the range of far-from equilibrium to local thermodynamic equilibrium conditions. The use of a detailed Collisional Radiative operator was necessary to accurately account for all processes of the collisional cascade during the relaxation of a hot plasma. To this end, the focus was in the development of (a) a detailed time accurate Collisional Radiative model, (b) a one-dimensional Multi-Fluid formulation that includes inelastic collisions, (c) a conservative BGK collision operator, and (d) hybridization techniques that blends low and high-fidelity algorithms.

The work performed over the last three years has done much to advance the state of the art in complexity reduction of Collisional Radiative (CR) modeling as well as the effects of inelastic collisions on the Multi-Fluid description of plasmas.

15. SUBJECT TERMS
Electric propulsion; plasma; collisional radiative; algorithms; argon; xenon; particle in cell; Monte Carlo method; Bhatnagar-Gross-Krook; BGK

16. SECURITY CLASSIFICATION OF:			**17. LIMITATION OF ABSTRACT**	**18. NUMBER OF PAGES**	**19a. NAME OF RESPONSIBLE PERSON**
					D. Bilyeu
a. REPORT	**b. ABSTRACT**	**c. THIS PAGE**			**19b. TELEPHONE NO** *(include area code)*
Unclassified	**Unclassified**	**Unclassified**	SAR	25	

Standard Form 298 (Rev. 8-98)
Prescribed by ANSI Std. 239.18

This Page Intentionally Left Blank

Table of Contents

List of Figures

List of Symbols, Abbreviations, and Acronyms

AFOSR	Air Force Office of Scientific Research
Ar	Argon
BGK	Bhatnagar-Gross-Krook
CR	collisional radiative
DSMC	direct simulation Monte Carlo
LANL	Los Alamos National Laboratory
LRIR	Laboratory Research Independent Research
NRL	Naval Research Laboratory
PIC	particle in cell

Q02Z Final Report: A Hybrid Model for Multiscale Laser Plasma Simulations with Detailed Collisional Physics

D. Bilyeu, PI
Air Force Research Laboratory
Edwards AFB, CA 93524, USA

May 11, 2017

The purpose of this document is to summarize the work accomplished under work unit Q02Z. The sole source of funding for this program was through AFOSR and was supported by Dr. Jason Marshall under contract 14RQ05COR and Dr. Fariba Fahroo under contract 12RZ06COR.

The overarching goals of this project was to develop a new numerical approach for multiscale plasma simulations that spans the range of far-from equilibrium to local thermodynamic equilibrium conditions. This is a very broad and ambitious goal and, in order to bring focus to this project, the plasma parameters were limited to those found in non-relativistic laser plasma interactions. The use of a detailed Collisional Radiative operator was necessary to accurately account for all processes of the collisional cascade during the relaxation of a hot plasma. To this end, the focus was in the development of

(a) a detailed time accurate Collisional Radiative model, (b) a one-dimensional Multi-Fluid formulation that includes inelastic collisions, (c) a conservative BGK collision operator, and (d) hybridization techniques that blends low and high-fidelity algorithms.

The work performed over the last three years has done much to advance the state of the art in complexity reduction of Collisional Radiative (CR) modeling as well as the effects of inelastic collisions on the Multi-Fluid description of plasmas. This work has been recognized in two workshop presentations, two conferences papers and five journal articles; four published [5, 6, 3, 7], and one awaiting review. The remainder of this report will summarize the accomplishments and techniques developed during this investigation.

1 Elastic Collisions and CR Models

Argon Collisional Radiative Modeling
The bulk of the work performed over the last three years focused on the extension of the CR model originally generated under a prior LRIR Task. In the previous LRIR task, a CR model with complexity reduction was derived and verified for atomic hydrogen. This investigation focuses on the extension of the previously derived algorithms to atoms with multiple ionization levels. This work was split between two successive goals. The first was to extend the current model to include multiple ionization levels without complexity reduction; this model was then validated

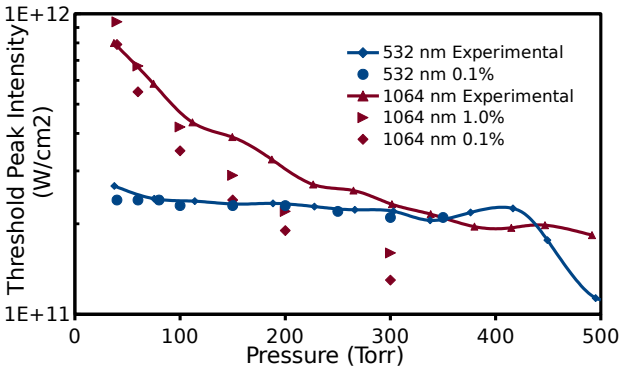

Figure 1: Pressure Vs. Breakdown intensity comparison with experimental results.

against experimental results as well as with code-to-code comparison. The second goal was to introduce the complexity reduction utilizing both uniform and Boltzmann grouping techniques. The Boltzmann and uniform grouping techniques were then compared against one another. The algorithms and corresponding code are generic and valid for all single atomic species but argon was used for all of the test cases. The choice of argon was due to the availability of a complete set of collisional cross-section and radiative data, made available through the Los Alamos National Labs (LANL) database[2, 4]. Argon presence in a wide range of interests (e.g., Field Reverse Configuration Thruster, LPI experiments) was also a contributing factor in its selection.

For the experimental comparison the code was compared against experiments from Sircar[8], shown in Figure 1. In this experiment the laser power required for breakdown to occur was measured under various background pressures. The main difficulty encountered during simulation was to define when breakdown occurred during the simulation and correlating the results to the experimentally determined breakdown values. Historically, a peak ionization fraction of 0.1% is used. Adopting the 0.1% convention resulted in good agreement for the 532 nm laser case. While a similar trend was observed for the 1064 nm case, the numerical result deviates for higher pressure scenarios. This deviation was most likely due to ionization potential depression or continuum lowering which was not accounted for in the code. This simulation also included the first two ionization levels of argon for a total of 633 excited states, 101 for Ar, 194 for Ar+ and 338 Ar++. To accurately capture the various CR processes required modeling several elementary processes including electron impact excitation/de-excitation, electron impact ionization/recombination, elastic collisions, radiation losses due to bound-bound transitions and bound-free processes, and laser based processes including multi-photon ionization and inverse Bremsstrahlung. One key physical process not included is radiation transfer; instead an optical escape factor is used to model the loss of energy due to radiation.

The second benchmark case compares our code against FLYCHK, a CR code created at Lawrence Livermore National Labs[1]. The ionization level vs the electron temperature was used to compare the two codes as shown in Figure 2. The electron temperature varied from 1 to 1000 eV and three different number densities, 10^{14}, 10^{20}, and 10^{23} cm^{-3}, were used. Overall, the two codes produced similar results. The largest discrepancies occurred with the high density case at low temperatures and the low density case at high temperature. For the high density low temperature case, the difference is likely due to corrections added to FLYCHK that account for high density effects such

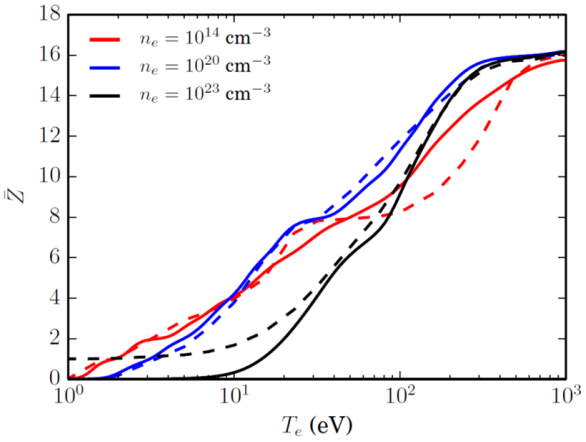

Figure 2: Comparison of equilibrium average ionization between FLYCHK (dashed) and AFRL (solid) argon CR solvers.

as continuum lowering. For the high temperature low density case, radiative recombination rates dominate three-body collisional deexcitation which establishes equilibrium, which then increases the sensitivity of the cross section data. Because the two codes use different sets of atomic data, discrepancies in this regime are not unexpected. It is also important to note that this is a code-to-code comparison and the validation of these simulations is an area of active research in the non-local thermodynamic equilibrium physics community.

The change from atomic hydrogen to argon required updating the code base to allow for non-analytical cross sections. During the initial investigation it was discovered that the argon system was much stiffer and a new ODE solver was required for an efficient and accurate solution. The Radau5 ODE integration solver was selected. This solver uses a 3-stage 5th order implicit Runge-Kutta scheme with adaptive time stepping. This method allows for an optimum time step to be selected, which was an improvement over the constant time step that the backwards Euler method used.

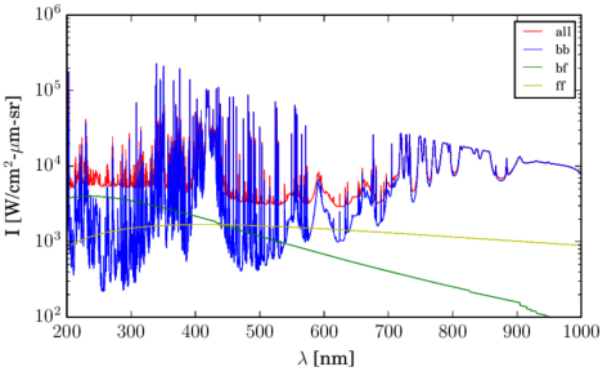

Figure 3: Example argon spectra.

Another improvement made to the CR model is the ability to compute a line-by-line radiation spectra from the CR rates, as shown in Figure 3. The current algorithm uses the CR model to generate the non-equilibrium population of the excited states, this in turn is used to determine the

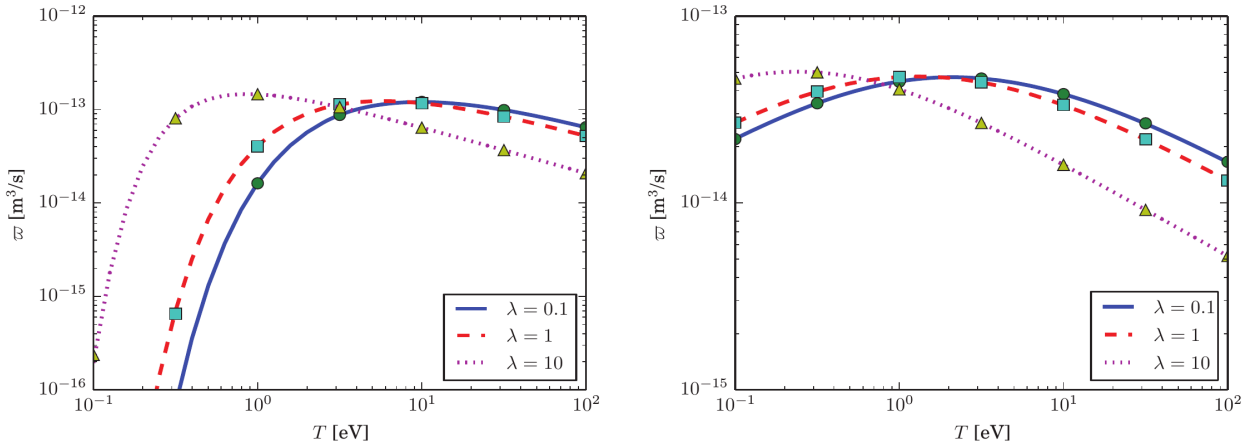

(a) Excitation ($2 \rightarrow 5$)

(b) Deexcitation ($2 \leftarrow 5$)

Figure 4: Comparison of zeroth-order reaction rate with Monte Carlo integration of the full transfer integral, where $\lambda = \frac{T_w}{T_e}$. A higher λ indicates a larger disparity between the kinetic energy between the two species.

emission and absorption coefficients. From this data the radiation spectra is generated and a plot of intensity versus wave number is generated. This spectra data serves a very useful validation tool because the computationally generated spectra can be directly compared to experimental results. Conversely this also provides experimentalists with a diagnostics tool that can produce spectral data for cases in which the excited states have not reached an equilibrium. Currently, the model assumes an optically thin plasma, which is only valid for low density plasmas, and this is a deficiency that should be addressed in the future.

Multi-Fluid Inelastic Collisions

For this investigation the CR model was extended to the Multi-Fluid regime. This involved the formulation of new exchange rates due to the drifting Maxwellian approximation. The results of this work has resulted in two published journal articles; the first covered excitation/de-excitation[5], and the second includes ionization and recombination[6]. The new algorithm is consistent with kinetic theory, has the correct asymptotic limits, and has microscopic detailed balance. The excitation/de-excitation results were compared to a Monte Carlo calculation, shown in Figure 4, and resulted in a very tight agreement. A similar comparison was done in the ionization/recombination paper and the Monte Carlo integration had excellent agreement with the full transfer integral[6]. A key finding during this investigation was the effect that the drift velocity has on the kinetics. Drift temperature is a convenient term to express the velocity difference between species and is expressed as,

$$T_w = \frac{\frac{1}{2}\frac{m_s m_t}{m_s + m_t}\left(u_s - u_t\right)^2}{k}.$$

This effect is shown in Figure 5. This figure shows two different results, one with an initial drift temperature of 0.01 eV and the other with an initial drift temperature of 10 eV. For each case the simulation was run both with and without the exchange terms due to inelastic collisions. For the 10 eV case the drift temperature is plotted in log-log scale beneath the semi-log plot containing a plot of the other temperatures. For both cases the total density is 10^{20} particles per cubic meter, the initial ionization fraction is 10% and the number density for the excited states is set to a small positive number, 10^{-15} particles per cubic meter.

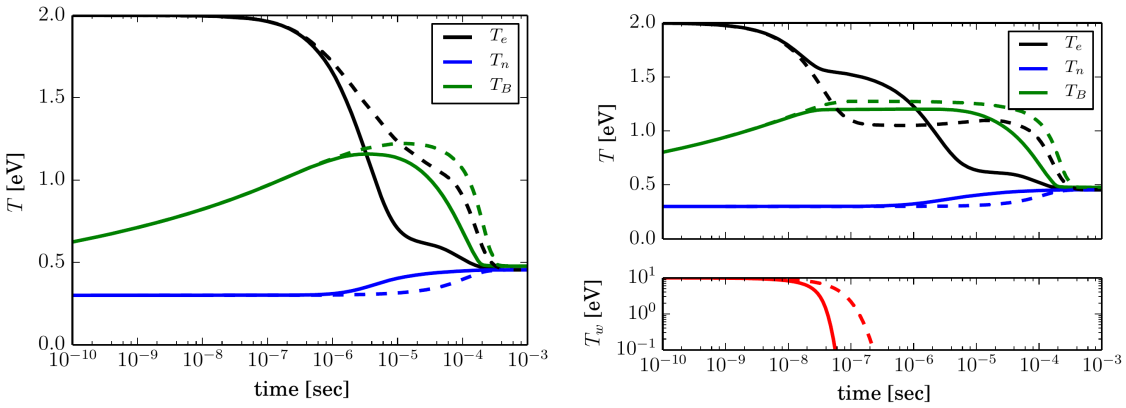

Figure 5: Time evolution of the temperatures for two different simulations are shown. Each simulation was run with (solid) and without (dashed) the exchange terms due to inelastic collisions. The plot on left starts with a T_w of 0.01 eV and the plots on the right starts at T_w of 10 eV. Both simulations have a total density of $10^{20}m^{-3}$ and an initial ionization fraction of 10%. The plot on the upper right shows the Boltzmann, electron, and neutral temperatures while the plot on the lower right shows the drift temperature in log-log scale.

This new algorithm is of particular relevance for laser-produced plasmas due to the large electric field produced either directly from the absorption process or via ponderomotive forces. This E-field creates an electron current which could impose and/or sustain the relative drift between the electrons and the heavy particles, which in turn impacts the rates. It was also discovered that the inelastic processes have an impact on the overall thermal equilibration process and should be included. These terms are typically not included in the standard collisional models.

2 Advanced PIC Algorithms

A new method to merge and split macro particles in PIC and DSMC codes was developed. This development started under AFOSR task, 12RZ06COR, and was completed under the current project. The findings were published in a journal article[7]. This method was designed to ensure conservation and to reduce thermalization there by preserving the velocity distribution function. The ability to control the number of macro particles in each cell is crucial to controlling the statistical error both locally and globally. Two situations in which this technique is useful are when new particles are generated (e.g. ionization) or when the density varies greatly throughout the domain (e.g. vacuum plume expansion).

As an example, consider an ionization breakdown simulation wherein a partially ionized flow is further ionized. A series of x-t plots comparing the electron number density and the computational particle count both with and without merging & splitting is shown as labeled on the top of Figure 6. This figure demonstrates the schemes ability to control the macro particle count while maintaining the correct physical number density. Figure 7 shows the computation cost versus the iteration count. When no merging and splitting is used the macro particle count grows at an exponential rate. Figures 6 and 7 shows that a significant time savings is gained through the merge & split algorithm without reducing the quality of the results.

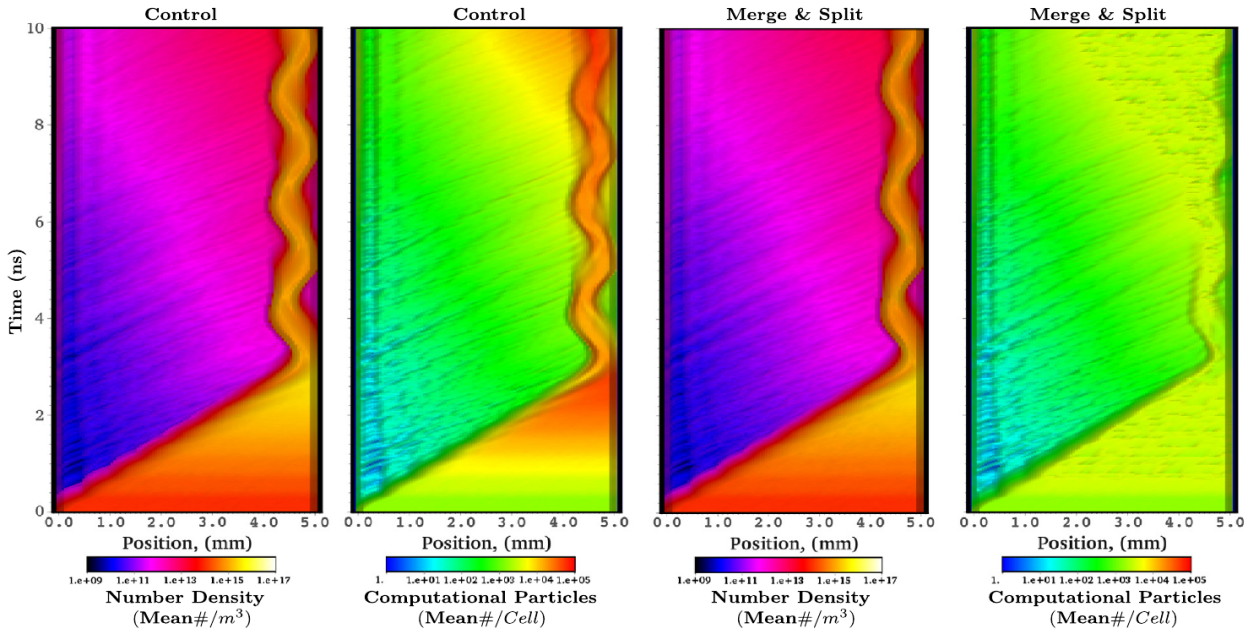

Figure 6: Physical and computational electron density during the ionizing breakdown case with and without merging and splitting for a 250 V potential from cathode (0 mm) to anode (5 mm) of each sub-figure. The case without merging is labeled as control.

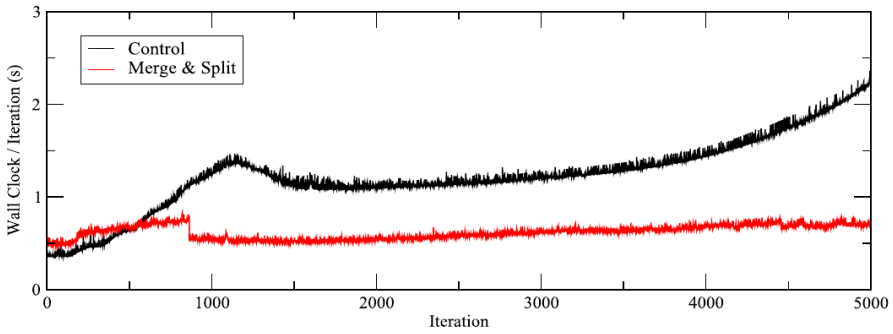

Figure 7: Computation cost during the ionizing breakdown case with and without merging and splitting for a 250 V potential from cathode to anode.

This work has been leveraged by another AFOSR task, 14RQ13COR, where this method was a critical component in a fractional Direct Simulation Monte Carlo (DSMC) collision algorithm. The fractional particle collision algorithm creates extra particles which can make these algorithms unusable but when combined with the octree merging algorithm the number of particles and computational cost can stay relatively constant.

3 Conservative BGK Integrator

One of the difficulties associated with multiscale simulations is the large number of time steps required for completion. During the course of a simulation errors can build up and can cause

numerical heating or cooling. Traditional BGK collisional operators exhibit these problems when multiple species are allowed to collide. Conservation becomes more of an issue as the mass ratio between the species increases, e.g. ion/electron systems. These issues led to the development of a new BGK collision operator. This method is fully conservative even when taking a time step larger than the collisional frequencies. A white paper containing the derivation and additional examples are included in Appendix A.

To test this algorithm, the relaxation of a plasma consisting of hot electrons and cold ions is shown in Figure 8. In this figure the same initial conditions are used but the problem is solved with different time steps. Although the rate of relaxation is different, the two solvers result in the correct equilibrium temperature.

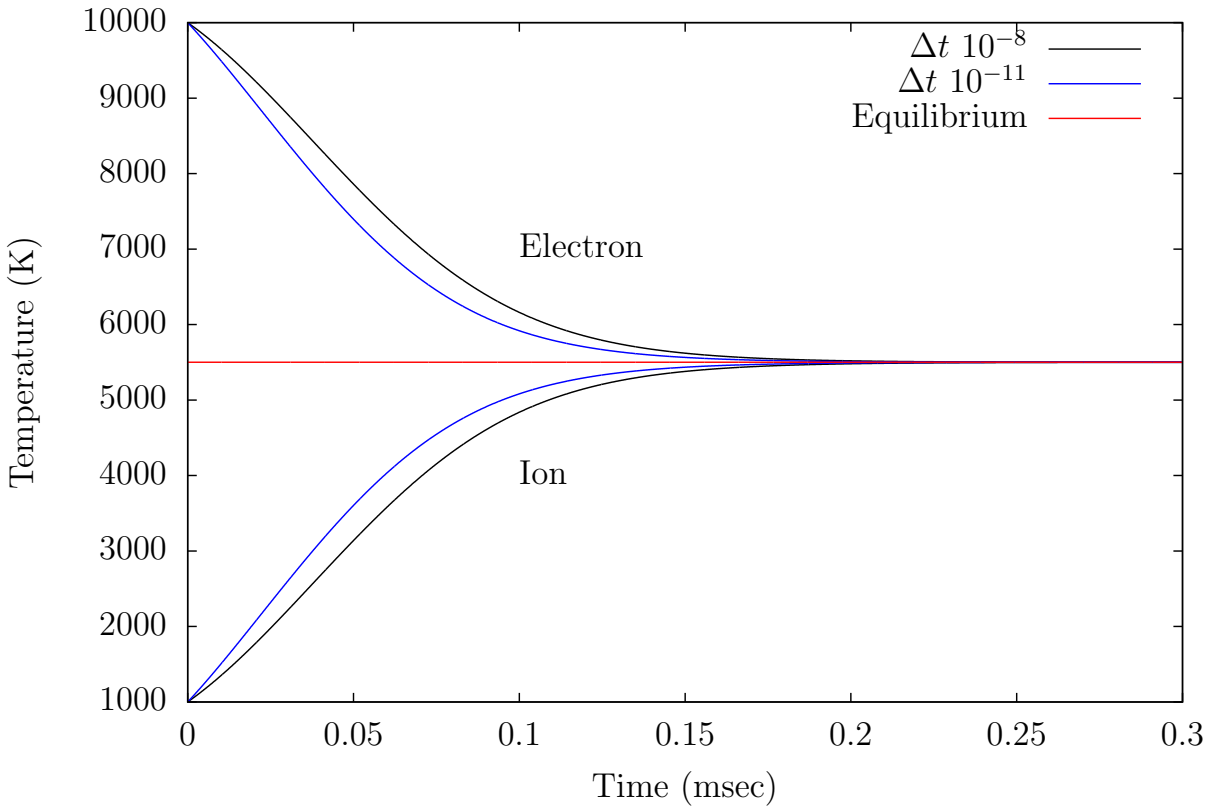

Figure 8: Impact of time integration scheme for BGK equilibration of electron-Ar^+ plasma.

This method could benefit through the addition of a velocity dependent collision frequency or by extending the algorithm to high order.

4 Multiscale Hybridization Techniques

The last topic investigated was the use hybridization techniques to address multiscale systems. When solving a physical system, there are typically multiple ways to model the physical system and each model can be solved using a variety of numerical algorithms. The techniques described in

this section seek to actively switch between different physical models; and/or numerical algorithms to efficiently solve a physical system. This new solver is intended to be more accurate than a coarse solution but not as numerically expensive as a fine grained solution. A paper detailing this method has been written and submitted to a journal for review.

For example, consider the motion of a charged particle in a magnetic field. Figure 9 solves this system using four different methods, Gyrokinetics, leapfrog PIC, a simple hybrid scheme, and by a modified time parallel method. The Gyrokinetics solver provides a coarse solution to the particle motion; it is computationally efficient but is expected to produce larger errors. The leapfrog PIC method requires a small time step for stability but produces a much more accurate solution and is used as our fine solution. The hybridization schemes represents two different physical models that governs the motion of the particle. The simple hybrid method uses an error estimator to determine which algorithm will be used to solve the system in the next time step. The time parallel method also uses an error estimator to select the solution method but also provides a blending zone wherein both solutions are solved [1]. Figure 9 plots the relative error compared to the computation time required to complete the simulation. For a given error level, the plot towards the left side represents the most computationally efficient method. Typically, a reduced time step provides more accurate solutions at the expense of increased computational time. The Gyrokinetics method has in the shortest computation time but its error doesn't improve beyond a certain level. This abrupt end to its accuracy is due to the physical limitations of the Gyrokinetic method. Though the leapfrog method converges to the lowest relative error, it is ten to a hundred times more computationally expensive than the time parallel method in the regions that the time parallel method was used. The simple hybrid method represents an improvement over the leapfrog method when the error is high but, just like the Gyrokinetic method, fails to improve as the computational effort increase. The time parallel method represents a good hybridization of the coarse and fine solvers. For a given error it is generally more accurate than the coarse solution and is always more computationally efficient than the fine solution.

[1] Note that although the time-parallel method can run in parallel all simulations were performed in serial.

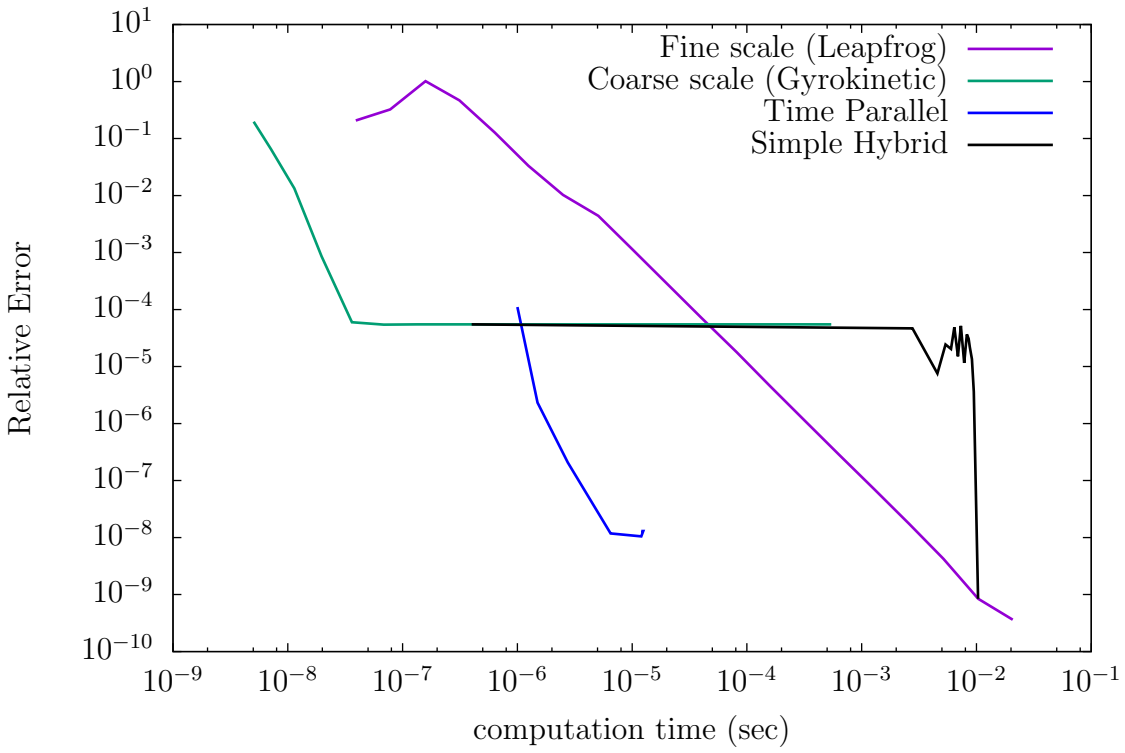

Figure 9: Relative error when computing the motion of a changed particle in a magnetic mirror

Moving forward, this technique will be applied to other problems of interest such as the hybridization of the Quasi Steady State method with the finite rate CR methods discussed earlier.

References

[1] Chung, H.-K., Chen, M., Morgan, W., Ralchenko, Y., and Lee, R. FLYCHK: Generalized population kinetics and spectral model for rapid spectroscopic analysis for all elements. *High Energy Density Physics 1* (2005), 3.

[2] Clark, R. E. H., Abdallah, J. J., and Mann, J. B. Integral and differential cross sections for electron impact ionization. *The Astrophysical Journal 381* (1991), 597–600.

[3] Lederman, C., Martin, R., Cambier, J. L., Time-parallel solutions to differential equations via functional optimization. *Comp. Appl. Math*, DOI 10.1007/s40314-016-0319-7 (2016).

[4] Colgan, J., Zhang, H. L., and Fontes, C. L. Electron-impact excitation and ionization cross sections for the si, cl, and ar isonuclear sequences. *Physics Review A 77*, 6 (2008).

[5] Le, H. P., and Cambier, J.-L. Modeling of inelastic collisions in a multifluid plasma: Excitation and deexcitation. *Physics of Plasmas (1994-present) 22*, 9 (2015), 093512.

[6] Le, H. P., and Cambier, J.-L. Modeling of inelastic collisions in a multifluid plasma: Ionization and Recombination. *Physics of Plasmas (1994-present) 23*, 6 (2016).

[7] Martin, R. S., and Cambier, J.-L. Octree particle management for dsmc and pic simulations. part i: Basic algorithms. *Journal of Computational Physics 327* (2016), 943–966.

[8] Sircar, A., Dwivedi, R. K., and Thareja, R. Laser Induced Breakdown of Ar, N2 and O2 Gasses Using 1.064, 0.532, 0.355 and 0.266 μm Radiation. *Applied Physics B 63*, 6 (1996), 623–627.

Appendix A Conservative BGK

A.1 Introduction

The Bhatnagar-Gross-Krook (BGK) model is a simplified collisional model that allows a particle distribution function to relax towards a equilibrium conditions at a rate defined by a collisional frequency. Although not as physically accurate as the full Boltzmann collisional integrals or the Fokker-Planck equation, its numerical efficiency and simplicity ensures its continued use in multi-dimensional kinetic simulations. Although the scheme is conservative by nature, the majority of the numerical implementations are unable to conserve the bulk properties, i.e., mass, momentum, and energy, of the gas. These numerical implementations only tend to preserve these quantities in the limit of an infinitely small time step. Furthermore, the schemes ability to conserve tend to diminish as the mass ratio of the gases increases, e.g., ion-electron.

A.2 Derivation

To begin consider the standard multi-component BGK operator,

$$\frac{Df_i}{Dt} = \sum_j^{N_S} \nu_{ij} \left(F_{ij} - f_i \right), \tag{1}$$

where f_i is the velocity distribution of the ith species, N_S is the total number of species present, F_{ij} is the Maxwellian of species i with respect to species j, and ν_{ij} is the collisional rate of species j with species i. For this investigation ν_{ij} assumed to be constant in velocity space. The Maxwellian has the form,

$$F_{ij}(\mathbf{v}, T_{ij}, \mathbf{u}_{ij}) = n_i \sqrt{\left(\frac{m_i}{2\pi K_b T_{ij}} \right)^{\mathcal{N}}} \exp\left(\frac{-m_i \left| \mathbf{v} - \mathbf{u}_{ij} \right|^2}{2K_b T_{ij}} \right) \tag{2}$$

where n_i and m_i are the number density and the mass of species i respectively, K_b is the Boltzmann constant and $\mathcal{N}$ is the number of velocity dimensions. T_{ij} and $\mathbf{u}_{ij}$ are the characteristic temperature and bulk velocity in $\mathcal{N}$ dimensions. The calculation of n_i, T_{ij} and $\mathbf{u}_{ij}$ will be detailed later. We can rewrite Eq. (1) as,

$$\frac{Df_i}{Dt} + \left(\sum_j^{N_S} \nu_{ij} \right) f_i = \sum_j^{N_S} \nu_{ij} F_{ij}. \tag{3}$$

For simplicity let $K_1^{(i)} \stackrel{\text{def}}{=} \sum_j^{N_S} \nu_{ij}$ and $K_2^{(i)} \stackrel{\text{def}}{=} \sum_j^{N_S} \nu_{ij} F_{ij}$. If we assume that ν_{ij} and F_{ij} are constant in time and defined at t^n then Eq. (1) has an analytical solution,

$$f_i(t) = f_i^n + \frac{1 - \exp\left(-\Delta t K_1^{(i)} \right)}{K_1^{(i)}} \left(K_2^{(i)} - K_1^{(i)} f_i^n \right), \tag{4}$$

where f_i^n is the distribution of f_i at time t^n and $\Delta t = t - t^n$. For simplicity let

$$A_a^{(i)} \stackrel{\text{def}}{=} \frac{1 - \exp\left(-\Delta t K_1^{(i)} \right)}{K_1^{(i)}}$$

then,

$$f_i(t) = f_i^n + A_a^{(i)} \left(K_2^{(i)} - K_1^{(i)} f_i^n \right). \tag{5}$$

As a side note Eq. (1) may also be solved through an Euler method

$$f_i(t) = f_i^n + A_E^{(i)}\left(K_2^{(i)} - K_1^{(i)} f_i^n\right)$$

where

$$A_E^{(i)} \stackrel{\text{def}}{=} \frac{\Delta t}{1 + \Delta t K_1^{(i)}(1-E)}, \quad E = \begin{cases} 0 & \text{implicit Euler} \\ 1/2 & \text{Crank-Nicolson} \\ 1 & \text{explicit Euler} \end{cases}$$

We return our attention to the bulk parameters, n_i, T_{ij}, and $\mathbf{u}_{ij}$. For the case when $j = i$ the bulk parameters are determined by taking the moments of the distribution function f_i at time t^n,

$$\begin{aligned} n_i &= \int_{\mathbf{v}} f_i^n d\mathbf{v}, \\ \mathbf{u}_{ii} = \mathbf{u}_i &= \frac{1}{n_i}\int_{\mathbf{v}} \mathbf{v} f_i^n d\mathbf{v}, \\ T_{ii} = T_i &= \frac{1}{K_b \mathcal{N}}\left(\frac{m_i}{n_i}\int_{\mathbf{v}} |\mathbf{v}|^2 f_i^n d\mathbf{v} - m_i|\mathbf{u}|^2\right) \end{aligned} \tag{6}$$

The values of T_{ij} and $\mathbf{u}_{ij}$ when $j \neq i$ are found by enforcing momentum and energy conservation. Momentum is conserved by enforcing,

$$\sum_i^{N_S} m_i \int_{\mathbf{v}} f_i(t)\mathbf{v} d\mathbf{v} = \text{ Constant.} \tag{7}$$

Enforcing this over a single time step yields,

$$\sum_i^{N_S} m_i \int_{\mathbf{v}} f_i(t^n + \Delta t)\mathbf{v} d\mathbf{v} = \sum_i^{N_S} m_i \int_{\mathbf{v}} f_i(t^n)\mathbf{v} d\mathbf{v} \tag{8}$$

or substituting Eq. (5) into Eq. (8)

$$\sum_i^{N_S} m_i \int_{\mathbf{v}} \left(f_i^n + A_a^{(i)}\left(K_2^{(i)} - K_1^{(i)} f_i^n\right)\right)\mathbf{v} d\mathbf{v} = \sum_i^{N_S} m_i \int_{\mathbf{v}} f_i(t^n)\mathbf{v} d\mathbf{v} \tag{9}$$

and then integrating over velocity

$$\sum_i^{N_S} m_i n_i A_a^{(i)}\left(\sum_j^{N_S} \nu_{ij}\mathbf{u}_{ij} - \mathbf{u}_i \sum_j^{N_S} \nu_{ij}\right) = 0. \tag{10}$$

Eq. (10) represents one equation and $(N_S - 1)N_S$ unknowns, so additional constraints are required. We enforce that as time advances all species approach the same velocity, i.e., $\mathbf{u}_{ij} = \bar{\mathbf{u}}$, for $j \neq i$. With this added constraint Eq. (10) can be solved for $\bar{\mathbf{u}}$,

$$\bar{\mathbf{u}} = \frac{\sum_i^{N_S} m_i A_a^{(i)} n_i \mathbf{u}_i \left(K_1^{(i)} - \nu_{ii}\right)}{\sum_i^{N_S} m_i A_a^{(i)} n_i \left(K_1^{(i)} - \nu_{ii}\right)}. \tag{11}$$

T_{ij} is determined by enforcing energy conservation over a time step,

$$\sum_i^{N_S} m_i \int_{\mathbf{v}} f_i(t^n + \Delta t)|\mathbf{v}|^2 d\mathbf{v} = \sum_i^{N_S} m_i \int_{\mathbf{v}} f_i(t^n)|\mathbf{v}|^2 d\mathbf{v}. \tag{12}$$

By following the same steps as in the momentum conservation and by assuming that all species will equilibrate towards the same temperature, $T_{ij} = \bar{T}$ for $j \neq i$, yields,

$$\bar{T} = \frac{\sum_i^{N_S} n_i A_a^{(i)}\left(K_1^{(i)} - \nu_{ii}\right)\left(\mathcal{N} K_b T_i + m_i\left(|\mathbf{u}_i|^2 - |\bar{\mathbf{u}}|^2\right)\right)}{\mathcal{N} K_b \sum_i^{N_S} n_i A_a^{(i)}\left(K_1^{(i)} - \nu_{ii}\right)}. \tag{13}$$

Substituting Eq. (11) and Eq. (13) into Eq. (2) yields,

$$F_{ij}(\mathbf{v},\bar{T},\bar{\mathbf{u}}) = n_i\sqrt{\left(\frac{m_i}{2\pi K_b\bar{T}}\right)^{\mathcal{N}}}\exp\left(\frac{-m_i\left|\mathbf{v}-\bar{\mathbf{u}}\right|^2}{2K_b\bar{T}}\right), j\neq i. \tag{14}$$

It should be noted that applying conservation of mass does not provide any useful relationships because the only terms present are the mass and number density of each species. This is easily shown by taking the zeroth moment,

$$\begin{aligned}\sum_i^{N_S} m_i\int_{\mathbf{v}} f_i(t^n+\Delta t)d\mathbf{v} &= \sum_i^{N_S} m_i\int_{\mathbf{v}} f_i(t^n)d\mathbf{v}\\ \sum_i^{N_S} m_i n_i &= \sum_i^{N_S} m_i n_i.\end{aligned} \tag{15}$$

This derivation was done for an arbitrary number of species, but in practice it is much more common to have only one or two specie present. As such the following equations are a simplification of the above assuming that only two species, a and b are present.

$$\begin{aligned}\frac{Df_a}{Dt} &= \nu_{aa}F_{aa}+\nu_{ab}F_{ab}-(\nu_{aa}+\nu_{ab})f_a,\\ \frac{Df_b}{Dt} &= \nu_{bb}F_{bb}+\nu_{ba}F_{ba}-(\nu_{bb}+\nu_{ba})f_b,\\ f_a(t) &= f_a^n + A\left(v_{aa}F_{aa}+v_{ab}F_{ab}-(v_{aa}+v_{ab})f_a^n\right),\\ f_b(t) &= f_b^n + A\left(v_{bb}F_{bb}+v_{ba}F_{ba}-(v_{bb}+v_{ba})f_b^n\right),\\ \bar{\mathbf{u}} &= \frac{m_a n_a\nu_{ab}A_a^{(a)}\mathbf{u}_a + m_b n_b\nu_{ba}A_a^{(b)}\mathbf{u}_b}{m_a n_a\nu_{ab}A_a^{(a)} + m_b n_b\nu_{ba}A_a^{(b)}},\\ \bar{T} &= \frac{n_a\nu_{ab}A_a^{(a)}\left(K_bT_a+m_a(|\mathbf{u}_a|^2-|\bar{\mathbf{u}}|^2)\right)+n_b\nu_{ba}A_a^{(b)}\left(K_bT_b+m_b(|\mathbf{u}_b|^2-|\bar{\mathbf{u}}|^2)\right)}{K_b\left(m_a n_a\nu_{ab}A_a^{(a)}+m_b n_b\nu_{ba}A_a^{(b)}\right)}.\end{aligned}$$

F_{aa}, F_{ab}, F_{bb}, and F_{ba} are easily computed from Eq. (2) and Eq. (14).

It is worthwhile to draw attention to several facts about this new derivation,

- The selection of the collisional rates are independent of each other, and does not affect conservation.
- No special treatment is required if both ions and electrons are present in the plasma to ensure conservation.
- Ensuring that mass, momentum, and energy are equal at t^n and $t^n+\Delta t$, is a weaker requirement than enforcing $\frac{\partial}{\partial t}\int_{\mathbf{v}} f(t)\mathbf{v}^{0,1,2}d\mathbf{v}=0$, but the later method does not have an analytical solution.
- The only difference between the analytical solution, implicit Euler, explicit Euler, and Crank-Nicolson methods is in the initial evaluation of A_a and A_E.
- T_i and $\mathbf{u}_i$ are also functions of time and can be evaluated at $t^n+\Delta t$ with out numerically integrating over velocity space.

A.3 Numerical Results

This section demonstrates the schemes ability to conserve mass, momentum, and energy by applying the new scheme to two different test cases. The first test consists relaxation of both temperature and bulk velocity for Argon and Xenon ions in three-dimensional velocity space. The second case shows temperature relaxation between Argon ions and electrons; this test case is performed with one velocity dimension. These test cases will show that mass, momentum, and energy are conserved to machine precision and that the entropy of the system increases in time. The results will also show that the temperature and bulk velocity relaxes towards the correct equilibrium conditions.

The collisional frequencies used in this investigation were obtained from the NRL plasma formulary with a small change for use with the mks system and to enforce a slower relaxation of the ions,

$$\begin{aligned}
\nu_{ee} \approx \nu_{\perp\ fast}^{e|e} &= 7.7 \times 10^{-12} n_e \lambda_{ee} \mathcal{T}_e^{-3/2}, \\
\nu_{ei} \approx \nu_{s\ fast}^{e|i} &= 3.9 \times 10^{-12} n_i \lambda_{ei} \mathcal{T}_{ei}^{-3/2}, \\
\nu_{ii} \approx \nu_{\perp\ slow}^{i|i} &= 1.8 \times 10^{-13} n_i \lambda_{ii} z^4 \mathcal{T}_i^{-3/2} (m_i/m_p)^{-1/2}, \\
\nu_{ie} &= m_e n_e v_{ei} / (m_i n_i) \\
\nu_{ab} \approx \nu_{s\ slow}^{i|i'} &= 6.8 \times 10^{-14} n_b z_a^2 z_b^2 \lambda_{ab} \mathcal{T}_{ab}^{-3/2} \frac{m_a}{m_b} \left(\frac{m_p}{m_a + m_b} \right)^{1/2}, \\
\mathcal{T}_{ab} = \mathcal{T}_{ba} &= \frac{\mathcal{T}_a m_b + \mathcal{T}_b m_a}{m_a + m_b},
\end{aligned} \tag{16}$$

where $\mathcal{T}$ is equal to the temperature in eV, m_p is the mass of a proton, and z is the unit charge of the ion. ν_{ab} is for ion-ion collisions where $a \neq b$. The Coulomb logarithm for all cases is equal to,

$$\begin{aligned}
\lambda &= \ln\left(4\pi n_e \lambda_D^3\right), \\
\lambda_D &= \sqrt{\frac{\varepsilon_0 K_B / q_e^2}{\sum_i^{N_S} z_i^2 n_i / T_i}}
\end{aligned} \tag{17}$$

where ε_0 is the permittivity of free space and q_e is the charge of an electron.

A.3.1 Argon-Xenon Thermal and Momentum Equilibrium

For this test case we consider the following initial conditions for Argon: $n = 2.5 \times 10^{19}$ $(1/m^3)$, $T = 1000$ (Kelvin), $\mathbf{u} = (1000, 0, 0)$ (m/s), and $z = 1$ (electron charge). And Xenon: $n = 2.5 \times 10^{19}$ $(1/m^3)$, $T = 10000$ (Kelvin), $\mathbf{u} = (-1000, 0, 0)$ (m/s), and $z = 1$ (electron charge). Velocity space is bounded at $\pm 2.5 \times 10^4$ (m/s) in all directions and the mesh spacing is 100 m/s in all directions. The simulation ran for 5 micro-seconds with a time step of 10 nano-seconds. The velocity bounds and spacing were selected such that the correct bulk properties, number density, velocity and temperature, were obtained at the start of the simulation. The equilibrium conditions are determined by enforcing momentum and energy conservation,

$$\begin{aligned}
\mathbf{u}_{eq} &= \frac{\sum_i^{N_S} \left(m_i n_i \mathbf{u}_i^0\right)}{\sum_i^{N_S} \left(m_i n_i\right)}, \\
T_{eq} &= \frac{\sum_i^{N_S} \mathcal{N} n_i K_B T_i^0 + m_i n_i |\mathbf{u}_i^0 - \mathbf{u}_{eq}|^2}{\sum_i^{N_S} \mathcal{N} n_i K_B},
\end{aligned} \tag{18}$$

where the superscript 0 represents the initial conditions and the subscript eq represents the equilibrium conditions. With these initial conditions the equilibrium velocity and temperature are,

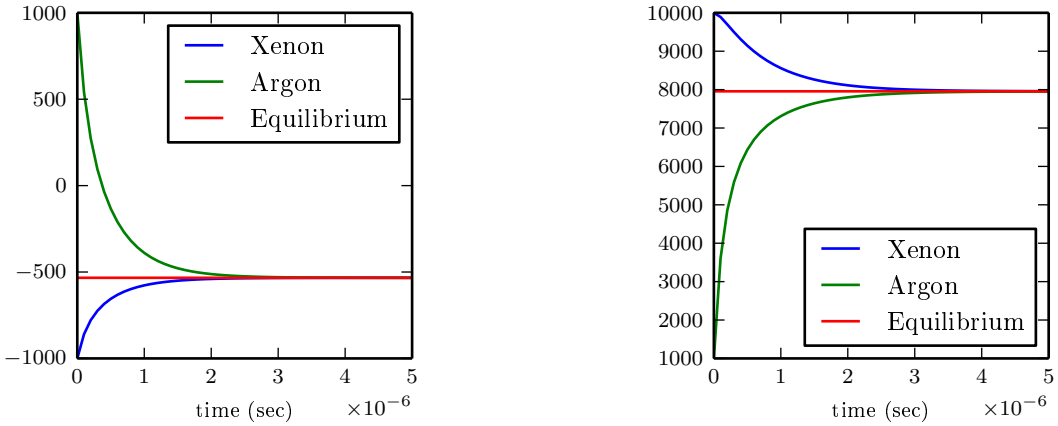

(a) Velocity (m/s)

(b) Temperature (Kelvin)

Figure A-1: Velocity and temperature time history for Argon-Xenon equilibration.

-533.421320034 m/s and 7955.8852308 Kelvin respectively. Figure A-1 shows that the correct equilibrium conditions are achieved, while the results shown in Fig. A-2 show that mass, momentum, and energy are conserved to machine precision and that entropy increases.

A.3.2 Argon Electron Thermal Equilibrium

For this test case we consider the following initial conditions for Argon: $n = 2.5 \times 10^{19}$ $(1/m^3)$, $T = 1000$ (Kelvin), $\mathbf{u} = 0$ (m/s), and $z = 1$ (electron charge). Velocity space for Argon is bounded at $\pm 5 \times 10^4$ m/s with a spacing of 250 m/s. The electrons have the following initial conditions, $n = 2.5 \times 10^{19}$ $(1/m^3)$, $T = 10000$ (Kelvin), and $\mathbf{u} = 0$ (m/s). Velocity space for the electrons is bounded at $\pm 1 \times 10^7$ m/s with a spacing of 50000 m/s. The simulation was performed using several time steps ranging from 10^{-8} to 10^{-11} and was allowed to run for 3×10^{-4} seconds. A typical simulation is shown in Figs A-3, and A-4, and used a time step of 10^{-10} seconds. In Fig. A-3 the time history of velocity and temperature for the Argon electron equilibration is shown; as expected the velocity of the two species stays near zero and the temperatures of the two gases approaches the correct equilibrium temperature of 5500 Kelvin. In Fig. A-4 the time history of the conservation bulk properties as well as the entropy are shown. The most likely cause for this is an accumulation of round off error, which is supported by the fact that the error per time step is around machine precision.

Even though the bulk properties are preserved the accuracy of the temperature and velocity profiles are affected by the time step. Figure A-5 shows the time history of the error in the ion temperature as well as the convergence rate of temperature. This plot shows the temperature convergence at a first order rate. This is not unexpected since it is assumed that the collisional frequency and the Maxwellian are constant during a time step, effectively a first order Taylor series expansion in time. It should be possible to increase the order of accuracy by expressing the collisional frequency and the Maxwellian as a higher order Taylor series in time. Also of note is that no analytical solution exists for this problem and the simulation was not run to convergence, thus the reference solution was chosen at a time step of 10^{-11} seconds.

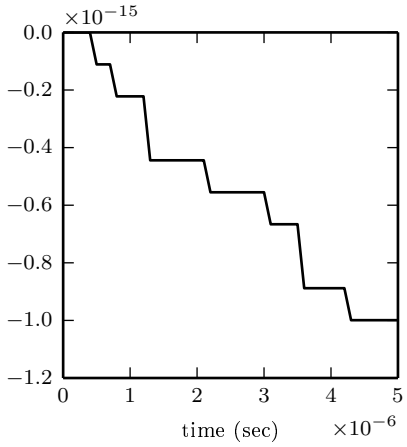

(a) Relative Mass Change

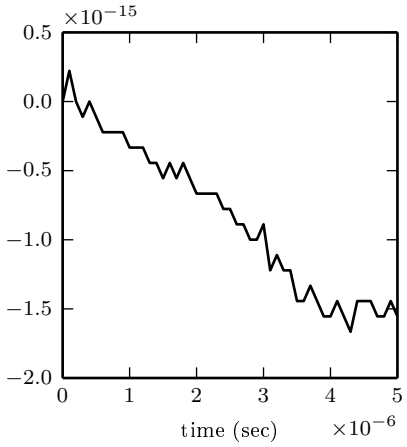

(b) Relative Momentum Change

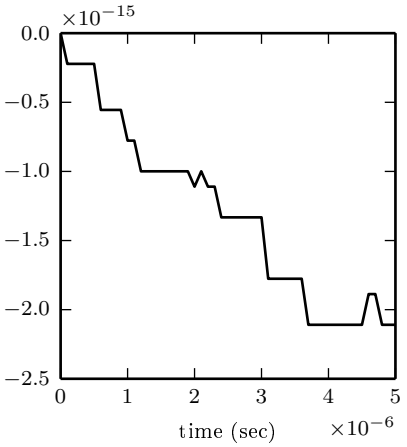

(c) Relative Energy Change

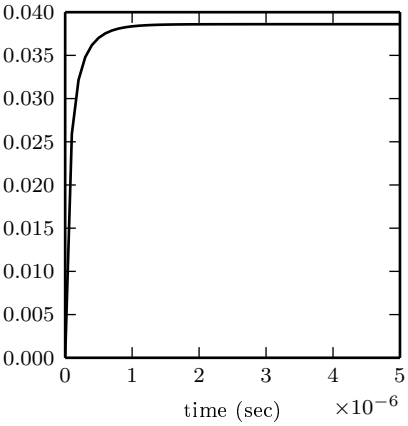

(d) Relative Entropy Change

Figure A-2: Time history plot of the conservation properties and entropy for Argon-Xenon equilibration.

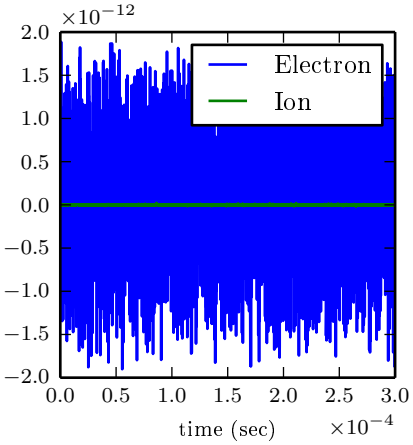

(a) Velocity (m/s)

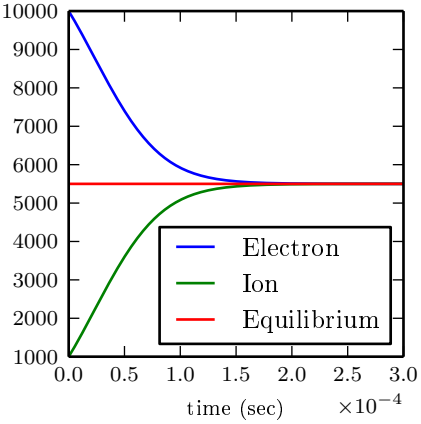

(b) Temperature (Kelvin)

Figure A-3: Velocity and temperature time history for Argon-electron equilibration.

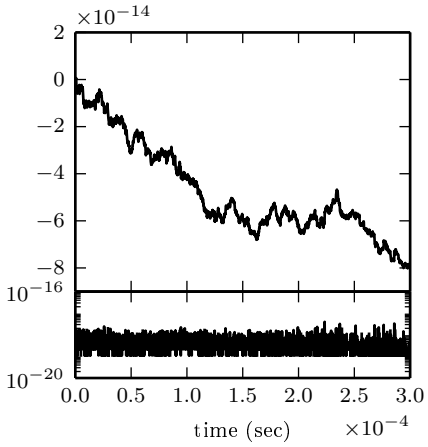

(a) Relative mass change

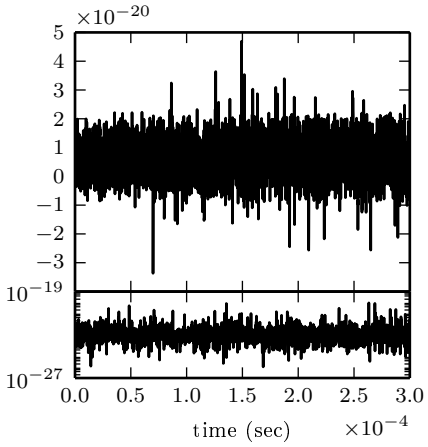

(b) Absolute momentum Change

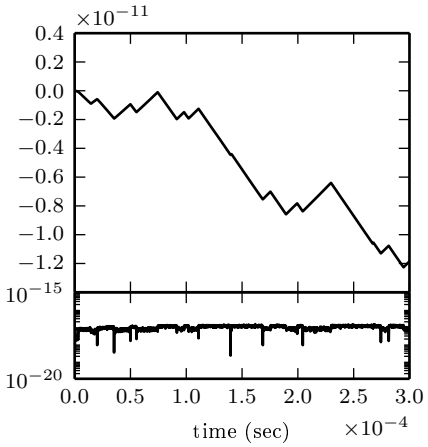

(c) Relative energy Change

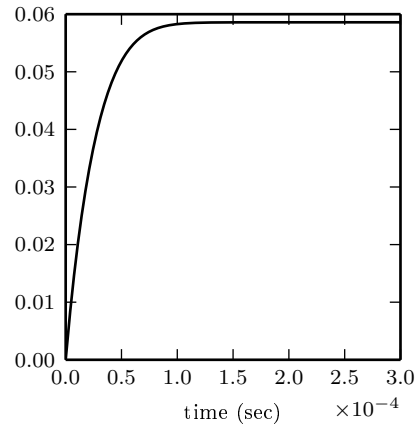

(d) Relative entropy Change

Figure A-4: Time history plot of the conservation properties and entropy for Argon-electron equilibration. For conservation plots the top is cumulative and bottom is per time step.

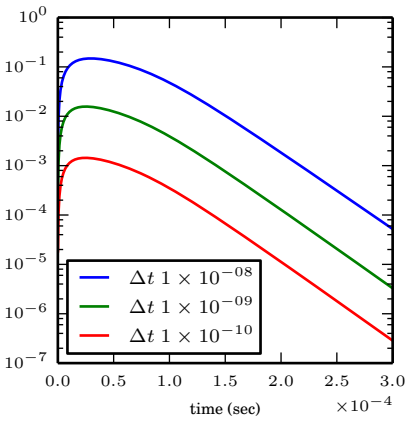

(a) Relative error in ion temperature

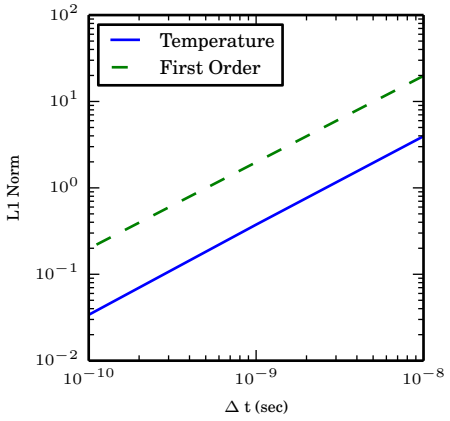

(b) Convergence rate for temperature

Figure A-5: Velocity and temperature time history for Argon-electron equilibration.

This Page Intentionally Left Blank

AFRL-RQ-ED-TR-2017-0012
Primary Distribution of this Report:

RQR
AFRL R&D Case Files
Completed Interim and Final Tech Reports Repository

AFRL/RQ Technical Library (2 CD + 1 HC)
6 Draco Drive
Edwards AFB, CA 93524-7130

Johns Hopkins University
Whiting School of Engineering
ATTN: Mary T. Gannaway/FSO
10630 Little Patuxent Pkwy, Suite 202
Columbia, MD 21044-3286

Defense Technical Information Center
(1 Electronic Submission via STINT)
Attn: DTIC-ACQS
8725 John J. Kingman Road, Suite 94
Ft. Belvoir, VA 22060-6218